Double parton interactions in $\gamma+3$ jet events in $p\bar{p}$ collisions at $\sqrt{s} = 1.96$ TeV

V.M. Abazov[37], B. Abbott[75], M. Abolins[64], B.S. Acharya[30], M. Adams[50], T. Adams[48], E. Aguilo[6], G.D. Alexeev[37], G. Alkhazov[41], A. Alton[64,a], G. Alverson[62], G.A. Alves[2], L.S. Ancu[36], M. Aoki[49], Y. Arnoud[14], M. Arov[59], A. Askew[48], B. Åsman[42], O. Atramentov[67], C. Avila[8], J. BackusMayes[82], F. Badaud[13], L. Bagby[49], B. Baldin[49], D.V. Bandurin[58], S. Banerjee[30], E. Barberis[62], A.-F. Barfuss[15], P. Baringer[57], J. Barreto[2], J.F. Bartlett[49], U. Bassler[18], D. Bauer[44], S. Beale[6], A. Bean[57], M. Begalli[3], M. Begel[73], C. Belanger-Champagne[42], L. Bellantoni[49], J.A. Benitez[64], S.B. Beri[28], G. Bernardi[17], R. Bernhard[23], I. Bertram[43], M. Besançon[18], R. Beuselinck[44], V.A. Bezzubov[40], P.C. Bhat[49], V. Bhatnagar[28], G. Blazey[51], S. Blessing[48], K. Bloom[66], A. Boehnlein[49], D. Boline[61], T.A. Bolton[58], E.E. Boos[39], G. Borissov[43], T. Bose[61], A. Brandt[78], R. Brock[64], G. Brooijmans[70], A. Bross[49], D. Brown[19], X.B. Bu[7], D. Buchholz[52], M. Buehler[81], V. Buescher[25], V. Bunichev[39], S. Burdin[43,b], T.H. Burnett[82], C.P. Buszello[44], P. Calfayan[26], B. Calpas[15], S. Calvet[16], E. Camacho-Pérez[34], J. Cammin[71], M.A. Carrasco-Lizarraga[34], E. Carrera[48], B.C.K. Casey[49], H. Castilla-Valdez[34], S. Chakrabarti[72], D. Chakraborty[51], K.M. Chan[55], A. Chandra[53], E. Cheu[46], S. Chevalier-Théry[18], D.K. Cho[61], S.W. Cho[32], S. Choi[33], B. Choudhary[29], T. Christoudias[44], S. Cihangir[49], D. Claes[66], J. Clutter[57], M. Cooke[49], W.E. Cooper[49], M. Corcoran[80], F. Couderc[18], M.-C. Cousinou[15], D. Cutts[77], M. Ćwiok[31], A. Das[46], G. Davies[44], K. De[78], S.J. de Jong[36], E. De La Cruz-Burelo[34], K. DeVaughan[66], F. Déliot[18], M. Demarteau[49], R. Demina[71], D. Denisov[49], S.P. Denisov[40], S. Desai[49], H.T. Diehl[49], M. Diesburg[49], A. Dominguez[66], T. Dorland[82], A. Dubey[29], L.V. Dudko[39], L. Duflot[16], D. Duggan[67], A. Duperrin[15], S. Dutt[28], A. Dyshkant[51], M. Eads[66], D. Edmunds[64], J. Ellison[47], V.D. Elvira[49], Y. Enari[17], S. Eno[60], H. Evans[53], A. Evdokimov[73], V.N. Evdokimov[40], G. Facini[62], A.V. Ferapontov[77], T. Ferbel[61,71], F. Fiedler[25], F. Filthaut[36], W. Fisher[64], H.E. Fisk[49], M. Fortner[51], H. Fox[43], S. Fuess[49], T. Gadfort[73], C.F. Galea[36], A. Garcia-Bellido[71], V. Gavrilov[38], P. Gay[13], W. Geist[19], W. Geng[15,64], D. Gerbaudo[68], C.E. Gerber[50], Y. Gershtein[67], D. Gillberg[6], G. Ginther[49,71], G. Golovanov[37], B. Gómez[8], A. Goussiou[82], P.D. Grannis[72], S. Greder[19], H. Greenlee[49], Z.D. Greenwood[59], E.M. Gregores[4], G. Grenier[20], Ph. Gris[13], J.-F. Grivaz[16], A. Grohsjean[18], S. Grünendahl[49], M.W. Grünewald[31], F. Guo[72], J. Guo[72], G. Gutierrez[49], P. Gutierrez[75], A. Haas[70,c], P. Haefner[26], S. Hagopian[48], J. Haley[62], I. Hall[64], L. Han[7], K. Harder[45], A. Harel[71], J.M. Hauptman[56], J. Hays[44], T. Hebbeker[21], D. Hedin[51], J.G. Hegeman[35], A.P. Heinson[47], U. Heintz[77], C. Hensel[24], I. Heredia-De La Cruz[34], K. Herner[63], G. Hesketh[62], M.D. Hildreth[55], R. Hirosky[81], T. Hoang[48], J.D. Hobbs[72], B. Hoeneisen[12], M. Hohlfeld[25], S. Hossain[75], P. Houben[35], Y. Hu[72], Z. Hubacek[10], N. Huske[17], V. Hynek[10], I. Iashvili[69], R. Illingworth[49], A.S. Ito[49], S. Jabeen[61], M. Jaffré[16], S. Jain[69], D. Jamin[15], R. Jesik[44], K. Johns[46], C. Johnson[70], M. Johnson[49], D. Johnston[66], A. Jonckheere[49], P. Jonsson[44], A. Juste[49,d], E. Kajfasz[15], D. Karmanov[39], P.A. Kasper[49], I. Katsanos[66], V. Kaushik[78], R. Kehoe[79], S. Kermiche[15], N. Khalatyan[49], A. Khanov[76], A. Kharchilava[69], Y.N. Kharzheev[37], D. Khatidze[77], M.H. Kirby[52], M. Kirsch[21], J.M. Kohli[28], A.V. Kozelov[40], J. Kraus[64], A. Kumar[69], A. Kupco[11], T. Kurča[20], V.A. Kuzmin[39], J. Kvita[9], D. Lam[55], S. Lammers[53], G. Landsberg[77], P. Lebrun[20], H.S. Lee[32], W.M. Lee[49], A. Leflat[39], J. Lellouch[17], L. Li[47], Q.Z. Li[49], S.M. Lietti[5], J.K. Lim[32], D. Lincoln[49], J. Linnemann[64], V.V. Lipaev[40], R. Lipton[49], Y. Liu[7], Z. Liu[6], A. Lobodenko[41], M. Lokajicek[11], P. Love[43], H.J. Lubatti[82], R. Luna-Garcia[34,e], A.L. Lyon[49], A.K.A. Maciel[2], D. Mackin[80], P. Mättig[27], R. Magaña-Villalba[34], P.K. Mal[46], S. Malik[66], V.L. Malyshev[37], Y. Maravin[58], J. Martínez-Ortega[34], R. McCarthy[72], C.L. McGivern[57], M.M. Meijer[36], A. Melnitchouk[65], L. Mendoza[8], D. Menezes[51], P.G. Mercadante[4], M. Merkin[39], A. Meyer[21], J. Meyer[24], N.K. Mondal[30], T. Moulik[57], G.S. Muanza[15], M. Mulhearn[81], O. Mundal[22], L. Mundim[3], E. Nagy[15], M. Naimuddin[29], M. Narain[77], R. Nayyar[29], H.A. Neal[63], J.P. Negret[8], P. Neustroev[41], H. Nilsen[23], H. Nogima[3], S.F. Novaes[5], T. Nunnemann[26], G. Obrant[41], D. Onoprienko[58], J. Orduna[34], N. Osman[44], J. Osta[55], R. Otec[10], G.J. Otero y Garzón[1], M. Owen[45], M. Padilla[47], P. Padley[80], M. Pangilinan[77], N. Parashar[54], V. Parihar[77], S.-J. Park[24], S.K. Park[32], J. Parsons[70], R. Partridge[77], N. Parua[53], A. Patwa[73], B. Penning[49], M. Perfilov[39], K. Peters[45], Y. Peters[45], P. Pétroff[16], R. Piegaia[1], J. Piper[64], M.-A. Pleier[73], P.L.M. Podesta-Lerma[34,f], V.M. Podstavkov[49], M.-E. Pol[2], P. Polozov[38], A.V. Popov[40], M. Prewitt[80], D. Price[53], S. Protopopescu[73], J. Qian[63], A. Quadt[24], B. Quinn[65], M.S. Rangel[16], K. Ranjan[29], P.N. Ratoff[43], I. Razumov[40], P. Renkel[79], P. Rich[45], M. Rijssenbeek[72], I. Ripp-Baudot[19], F. Rizatdinova[76], S. Robinson[44], M. Rominsky[75], C. Royon[18], P. Rubinov[49], R. Ruchti[55], G. Safronov[38], G. Sajot[14], A. Sánchez-Hernández[34], M.P. Sanders[26], B. Sanghi[49], G. Savage[49], L. Sawyer[59], T. Scanlon[44], D. Schaile[26], R.D. Schamberger[72], Y. Scheglov[41], H. Schellman[52], T. Schliephake[27], S. Schlobohm[82], C. Schwanenberger[45], R. Schwienhorst[64], J. Sekaric[57], H. Severini[75], E. Shabalina[24], V. Shary[18], A.A. Shchukin[40], R.K. Shivpuri[29], V. Simak[10], V. Sirotenko[49], N.B. Skachkov[37],

P. Skubic[75], P. Slattery[71], D. Smirnov[55], G.R. Snow[66], J. Snow[74], S. Snyder[73], S. Söldner-Rembold[45],
L. Sonnenschein[21], A. Sopczak[43], M. Sosebee[78], K. Soustruznik[9], B. Spurlock[78], J. Stark[14], V. Stolin[38],
D.A. Stoyanova[40], J. Strandberg[63], M.A. Strang[69], E. Strauss[72], M. Strauss[75], R. Ströhmer[26], D. Strom[50],
L. Stutte[49], P. Svoisky[36], M. Takahashi[45], A. Tanasijczuk[1], W. Taylor[6], B. Tiller[26], M. Titov[18], V.V. Tokmenin[37],
D. Tsybychev[72], B. Tuchming[18], C. Tully[68], P.M. Tuts[70], R. Unalan[64], L. Uvarov[41], S. Uvarov[41], S. Uzunyan[51],
P.J. van den Berg[35], R. Van Kooten[53], W.M. van Leeuwen[35], N. Varelas[50], E.W. Varnes[46], I.A. Vasilyev[40],
P. Verdier[20], A.Y. Verkheev[37], L.S. Vertogradov[37], M. Verzocchi[49], M. Vesterinen[45], D. Vilanova[18], P. Vint[44],
P. Vokac[10], H.D. Wahl[48], M.H.L.S. Wang[71], J. Warchol[55], G. Watts[82], M. Wayne[55], G. Weber[25], M. Weber[49,g],
M. Wetstein[60], A. White[78], D. Wicke[25], M.R.J. Williams[43], G.W. Wilson[57], S.J. Wimpenny[47], M. Wobisch[59],
D.R. Wood[62], T.R. Wyatt[45], Y. Xie[49], C. Xu[63], S. Yacoob[52], R. Yamada[49], W.-C. Yang[45], T. Yasuda[49],
Y.A. Yatsunenko[37], Z. Ye[49], H. Yin[7], K. Yip[73], H.D. Yoo[77], S.W. Youn[49], J. Yu[78], C. Zeitnitz[27], S. Zelitch[81],
T. Zhao[82], B. Zhou[63], J. Zhu[72], M. Zielinski[71], D. Zieminska[53], L. Zivkovic[70], V. Zutshi[51], and E.G. Zverev[39]

(The DØ Collaboration)

[1] *Universidad de Buenos Aires, Buenos Aires, Argentina*
[2] *LAFEX, Centro Brasileiro de Pesquisas Físicas, Rio de Janeiro, Brazil*
[3] *Universidade do Estado do Rio de Janeiro, Rio de Janeiro, Brazil*
[4] *Universidade Federal do ABC, Santo André, Brazil*
[5] *Instituto de Física Teórica, Universidade Estadual Paulista, São Paulo, Brazil*
[6] *Simon Fraser University, Burnaby, British Columbia,*
Canada; and York University, Toronto, Ontario, Canada
[7] *University of Science and Technology of China, Hefei, People's Republic of China*
[8] *Universidad de los Andes, Bogotá, Colombia*
[9] *Center for Particle Physics, Charles University,*
Faculty of Mathematics and Physics, Prague, Czech Republic
[10] *Czech Technical University in Prague, Prague, Czech Republic*
[11] *Center for Particle Physics, Institute of Physics,*
Academy of Sciences of the Czech Republic, Prague, Czech Republic
[12] *Universidad San Francisco de Quito, Quito, Ecuador*
[13] *LPC, Université Blaise Pascal, CNRS/IN2P3, Clermont, France*
[14] *LPSC, Université Joseph Fourier Grenoble 1, CNRS/IN2P3,*
Institut National Polytechnique de Grenoble, Grenoble, France
[15] *CPPM, Aix-Marseille Université, CNRS/IN2P3, Marseille, France*
[16] *LAL, Université Paris-Sud, IN2P3/CNRS, Orsay, France*
[17] *LPNHE, IN2P3/CNRS, Universités Paris VI and VII, Paris, France*
[18] *CEA, Irfu, SPP, Saclay, France*
[19] *IPHC, Université de Strasbourg, CNRS/IN2P3, Strasbourg, France*
[20] *IPNL, Université Lyon 1, CNRS/IN2P3, Villeurbanne, France and Université de Lyon, Lyon, France*
[21] *III. Physikalisches Institut A, RWTH Aachen University, Aachen, Germany*
[22] *Physikalisches Institut, Universität Bonn, Bonn, Germany*
[23] *Physikalisches Institut, Universität Freiburg, Freiburg, Germany*
[24] *II. Physikalisches Institut, Georg-August-Universität Göttingen, Göttingen, Germany*
[25] *Institut für Physik, Universität Mainz, Mainz, Germany*
[26] *Ludwig-Maximilians-Universität München, München, Germany*
[27] *Fachbereich Physik, University of Wuppertal, Wuppertal, Germany*
[28] *Panjab University, Chandigarh, India*
[29] *Delhi University, Delhi, India*
[30] *Tata Institute of Fundamental Research, Mumbai, India*
[31] *University College Dublin, Dublin, Ireland*
[32] *Korea Detector Laboratory, Korea University, Seoul, Korea*
[33] *SungKyunKwan University, Suwon, Korea*
[34] *CINVESTAV, Mexico City, Mexico*
[35] *FOM-Institute NIKHEF and University of Amsterdam/NIKHEF, Amsterdam, The Netherlands*
[36] *Radboud University Nijmegen/NIKHEF, Nijmegen, The Netherlands*
[37] *Joint Institute for Nuclear Research, Dubna, Russia*
[38] *Institute for Theoretical and Experimental Physics, Moscow, Russia*
[39] *Moscow State University, Moscow, Russia*
[40] *Institute for High Energy Physics, Protvino, Russia*
[41] *Petersburg Nuclear Physics Institute, St. Petersburg, Russia*
[42] *Stockholm University, Stockholm, Sweden, and Uppsala University, Uppsala, Sweden*
[43] *Lancaster University, Lancaster, United Kingdom*

[44] *Imperial College London, London SW7 2AZ, United Kingdom*
[45] *The University of Manchester, Manchester M13 9PL, United Kingdom*
[46] *University of Arizona, Tucson, Arizona 85721, USA*
[47] *University of California, Riverside, California 92521, USA*
[48] *Florida State University, Tallahassee, Florida 32306, USA*
[49] *Fermi National Accelerator Laboratory, Batavia, Illinois 60510, USA*
[50] *University of Illinois at Chicago, Chicago, Illinois 60607, USA*
[51] *Northern Illinois University, DeKalb, Illinois 60115, USA*
[52] *Northwestern University, Evanston, Illinois 60208, USA*
[53] *Indiana University, Bloomington, Indiana 47405, USA*
[54] *Purdue University Calumet, Hammond, Indiana 46323, USA*
[55] *University of Notre Dame, Notre Dame, Indiana 46556, USA*
[56] *Iowa State University, Ames, Iowa 50011, USA*
[57] *University of Kansas, Lawrence, Kansas 66045, USA*
[58] *Kansas State University, Manhattan, Kansas 66506, USA*
[59] *Louisiana Tech University, Ruston, Louisiana 71272, USA*
[60] *University of Maryland, College Park, Maryland 20742, USA*
[61] *Boston University, Boston, Massachusetts 02215, USA*
[62] *Northeastern University, Boston, Massachusetts 02115, USA*
[63] *University of Michigan, Ann Arbor, Michigan 48109, USA*
[64] *Michigan State University, East Lansing, Michigan 48824, USA*
[65] *University of Mississippi, University, Mississippi 38677, USA*
[66] *University of Nebraska, Lincoln, Nebraska 68588, USA*
[67] *Rutgers University, Piscataway, New Jersey 08855, USA*
[68] *Princeton University, Princeton, New Jersey 08544, USA*
[69] *State University of New York, Buffalo, New York 14260, USA*
[70] *Columbia University, New York, New York 10027, USA*
[71] *University of Rochester, Rochester, New York 14627, USA*
[72] *State University of New York, Stony Brook, New York 11794, USA*
[73] *Brookhaven National Laboratory, Upton, New York 11973, USA*
[74] *Langston University, Langston, Oklahoma 73050, USA*
[75] *University of Oklahoma, Norman, Oklahoma 73019, USA*
[76] *Oklahoma State University, Stillwater, Oklahoma 74078, USA*
[77] *Brown University, Providence, Rhode Island 02912, USA*
[78] *University of Texas, Arlington, Texas 76019, USA*
[79] *Southern Methodist University, Dallas, Texas 75275, USA*
[80] *Rice University, Houston, Texas 77005, USA*
[81] *University of Virginia, Charlottesville, Virginia 22901, USA and*
[82] *University of Washington, Seattle, Washington 98195, USA*
(Dated: March 1, 2010)

We have used a sample of $\gamma + 3$ jets events collected by the D0 experiment with an integrated luminosity of about 1 fb^{-1} to determine the fraction of events with double parton scattering ($f_{\rm DP}$) in a single $p\bar{p}$ collision at $\sqrt{s} = 1.96$ TeV. The DP fraction and effective cross section ($\sigma_{\rm eff}$), a process-independent scale parameter related to the parton density inside the nucleon, are measured in three intervals of the second (ordered in p_T) jet transverse momentum $p_T^{\rm jet2}$ within the range $15 \leq p_T^{\rm jet2} \leq 30$ GeV. In this range, $f_{\rm DP}$ varies between $0.23 \leq f_{\rm DP} \leq 0.47$, while $\sigma_{\rm eff}$ has the average value $\sigma_{\rm eff}^{\rm ave} = 16.4 \pm 0.3({\rm stat}) \pm 2.3({\rm syst})$ mb.

PACS numbers: 14.20Dh, 13.85.Qk, 13.87.Ce, 12.38.Qk

I. INTRODUCTION

Many features of high energy inelastic hadron collisions depend directly on the parton structure of hadrons. The inelastic scattering of nucleons need not to occur only through a single parton-parton interaction and the contribution from double parton (DP) collisions can be significant. A schematic view of a double parton scattering event in a $p\bar{p}$ interaction is shown in Fig. 1. The rate of events with multiple parton scatterings depends on how the partons are spatially distributed within the nucleon.

Theoretical discussions and estimations [1–5] stimulated measurements [6–9] of DP event fractions and DP cross sections. The latter can be expressed as

$$\sigma_{\rm DP} \equiv m\frac{\sigma_{\rm A}\sigma_{\rm B}}{2\sigma_{\rm eff}}, \quad (1)$$

where $\sigma_{\rm A}$ and $\sigma_{\rm B}$ are the cross sections of two independent partonic scatterings A and B. The factor m is equal to unity when processes A and B are indistinguishable while $m = 2$ otherwise [5, 10, 11]. The process-independent scaling parameter $\sigma_{\rm eff}$ has the units of cross
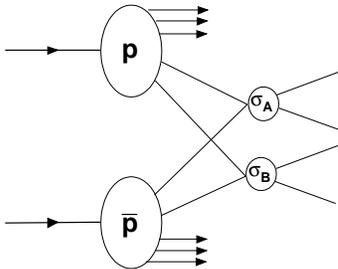
FIG. 1: Diagram of a double parton scattering event.

section. Its relation to the spatial distribution of partons within the proton has been discussed in [1, 3–5, 10, 11]. The ratio $\sigma_B/\sigma_{\text{eff}}$ can be interpreted as the probability for partonic process B to occur provided that process A has already occurred. If the partons are uniformly distributed inside the nucleon (large σ_{eff}), σ_{DP} will be rather small and, conversely, it will be large for a highly concentrated parton spatial density (small σ_{eff}). The implication and possible correlations of parton momenta distribution functions in (1) are discussed in [12–14].

In addition to constraining predictions from various models of nucleon structure and providing a better understanding of non-perturbative QCD dynamics, measurements of f_{DP} and σ_{eff} are also needed for the accurate estimation of backgrounds for many rare new physics processes as well as for Higgs boson searches at the Tevatron and LHC [15, 16].

To date, there have been only four dedicated measurements studying double parton scattering: by the AFS Collaboration in pp collisions at $\sqrt{s} = 63$ GeV [6], by the UA2 Collaboration in $p\bar{p}$ collisions at $\sqrt{s} = 630$ GeV [7], and twice by the CDF Collaboration in $p\bar{p}$ collisions at $\sqrt{s} = 1.8$ TeV [8, 9]. The four-jet final state was used in the measurements to extract values of σ_{DP} and then σ_{eff}, and the $\gamma + 3$ jets final state was used in [9] to extract f_{DP} fractions and then σ_{eff}. The obtained values of σ_{eff} by those experiments are $\sigma_{\text{eff}} \approx 5$ mb (AFS), $\sigma_{\text{eff}} > 8.3$ mb at the 95% C.L. (UA2), $\sigma_{\text{eff}} = 12.1^{+10.7}_{-5.4}$ mb (CDF, four-jet) and $\sigma_{\text{eff}} = 14.5 \pm 1.7^{+1.7}_{-2.3}$ mb (CDF, $\gamma + 3$ jets). Table I summarizes all previous measurements of σ_{eff}, σ_{DP}, and f_{DP}.

This paper presents an analysis of hard inelastic events with a photon candidate (denoted below as γ) and at least 3 jets (referred to below as "$\gamma + 3$ jets" events) collected with the D0 detector [17] at the Fermilab Tevatron Collider with $\sqrt{s} = 1.96$ TeV and an integrated luminosity of 1.02 ± 0.06 fb^{-1}. In this final state, DP events are caused by two partonic scatterings, with γ+jets production in the first scattering and dijet production in the second. Thus, the rate of $\gamma + 3$ jets events and their kinematics should be sensitive to a contribution from additional parton interactions. Differences in the types of the two final states (γ+jets and dijets) and better energy measurement of photons as compared with jets facilitate differentiation between the two DP scatterings as compared with the 4-jet measurements. Also, it was

shown in [18] that a larger fraction of DP events is expected in the $\gamma + 3$ jets final state as compared with the 4-jet events. The large integrated luminosity allows us to select $\gamma + 3$ jets events at high photon transverse momentum, $60 < p_T^{\gamma} < 80$ GeV (vs. $p_T^{\gamma} > 16$ GeV in CDF [9]), with a larger photon purity [19]. The choice of a high threshold on the photon momentum provides (a) a clean separation between the jet produced in the same parton scattering from which the photon originates and the jets originating from additional parton scatterings and (b) a better determination of the energy scale of the γ+jets process. Also, in contrast to [9], the jet transverse momenta are corrected to the particle level. Other differences in the technique used for extracting σ_{eff} are described below.

This paper is organized as follows. Section II briefly describes the technique used to extract the σ_{eff} parameter. Section III provides the description of the data samples and selection criteria. Section IV describes the models used for signal and background events. In Section V we introduce the variables which allow us to distinguish DP events from other $\gamma + 3$ jets events and determine their fraction. The procedure for finding the fractions of DP events is described in Section VI. Section VII describes the determination of other parameters needed to calculate σ_{eff}. Results of the measurement are given in Section VIII with their application to selected models of parton density.

II. TECHNIQUE FOR EXTRACTING σ_{eff} FROM DATA

In the 4-jet analyses [6–8], σ_{eff} was extracted from measured DP cross sections using Monte Carlo (MC) modeling for signal and background events and QCD predictions for the dijet cross sections. Both MC modeling and the QCD predictions suffer from substantial uncertainties leading to analogous uncertainties in σ_{eff}. Another technique for extracting σ_{eff} was proposed in [9]. It uses only quantities determined from data and thus minimizes the impact of theoretical assumptions. Here we follow this method and extract σ_{eff} without theoretical predictions of the $\gamma +$ jets and dijets cross sections by comparing the number of $\gamma + 3$ jets events produced in DP interactions in single $p\bar{p}$ collisions to the number of $\gamma + 3$ jets events produced in two distinct hard interactions occurring in two separate $p\bar{p}$ collisions in the same beam crossing. The latter class of events is referred to as double interaction (DI) events. Assuming uncorrelated parton scatterings in the DP process [1–5, 11], DP and DI events should be kinematically identical. This assumption is discussed in Appendix A.

Measurements of dijet production with jet $p_T \gtrsim 12 - 15$ GeV [20] in both central and forward rapidity [21] regions indicate that the contribution from single and double diffraction events represents $\lesssim 1\%$ of the total dijet cross section. Therefore $\gamma +$ jets and dijet events with jet

TABLE I: Summary of the results, experimental parameters, and event selections for the double parton analyses performed by the AFS, UA2 and CDF Collaborations.

Experiment	$\sqrt{s}$ (GeV)	Final state	p_T^{min} (GeV)	η range	σ_{eff}	σ_{DP}, f_{DP}
AFS (pp), 1986 [6]	63	4 jets	$p_T^{\text{jet}} > 4$	$|\eta^{\text{jet}}| < 1$	~ 5 mb	$\sigma_{\text{DP}}/\sigma_{\text{dijet}} = (6 \pm 1.5 \pm 2.0)\%$
UA2 ($p\bar{p}$), 1991 [7]	630	4 jets	$p_T^{\text{jet}} > 15$	$|\eta^{\text{jet}}| < 2$	> 8.3 mb (95% C.L.)	$\sigma_{\text{DP}} = 0.49 \pm 0.20$ nb
CDF ($p\bar{p}$), 1993 [8]	1800	4 jets	$p_T^{\text{jet}} > 25$	$|\eta^{\text{jet}}| < 3.5$	$12.1^{+10.7}_{-5.4}$ mb	$\sigma_{\text{DP}} = (63^{+32}_{-28})$ nb, $f_{\text{DP}} = (5.4^{+1.6}_{-2.0})\%$
CDF ($p\bar{p}$), 1997 [9]	1800	$\gamma + 3$ jets	$p_T^{\text{jet}} > 6$	$|\eta^{\text{jet}}| < 3.5$		
			$p_T^{\gamma} > 16$	$|\eta^{\gamma}| < 0.9$	$14.5 \pm 1.7^{+1.7}_{-2.3}$ mb	$f_{\text{DP}} = (52.6 \pm 2.5 \pm 0.9)\%$

$p_T > 15$ GeV are produced predominantly as a result of inelastic non-diffractive (hard) $p\bar{p}$ interactions. In a $p\bar{p}$ beam crossing with two hard collisions the probability for a DI event in that crossing can be expressed as

$$P_{\text{DI}} = 2 \frac{\sigma^{\gamma j}}{\sigma_{\text{hard}}} \frac{\sigma^{jj}}{\sigma_{\text{hard}}}. \qquad (2)$$

Here $\sigma^{\gamma j}$ and σ^{jj} are the cross sections to produce the inclusive $\gamma + $ jets and dijet events, which combined give the $\gamma + 3$ jets final state, and σ_{hard} is the total hard $p\bar{p}$ interaction cross section. The factor 2 takes into account that the two hard scatterings, producing a $\gamma + $jets or dijet event, can be ordered in two ways with respect to the two collision vertices in the DI events. The number of DI events, N_{DI}, can be obtained from P_{DI}, after correction for the efficiencies to pass geometric and kinematic selection criteria ϵ_{DI}, the two-vertex event selection efficiency, ϵ_{2vtx}, and the number of beam crossings with two hard collisions, N_{2coll}:

$$N_{\text{DI}} = 2 \frac{\sigma^{\gamma j}}{\sigma_{\text{hard}}} \frac{\sigma^{jj}}{\sigma_{\text{hard}}} N_{\text{2coll}} \, \epsilon_{\text{DI}} \, \epsilon_{\text{2vtx}}. \qquad (3)$$

Analogously to P_{DI}, the probability for DP events, P_{DP}, in a beam crossing with one hard collision, is

$$P_{\text{DP}} = \frac{\sigma_{\text{DP}}}{\sigma_{\text{hard}}} = \frac{\sigma^{\gamma j}}{\sigma_{\text{eff}}} \frac{\sigma^{jj}}{\sigma_{\text{hard}}}, \qquad (4)$$

where we used Eq. (1). Then the number of DP events, N_{DP}, can be expressed from P_{DP} with a correction for the geometric and kinematic selection efficiency ϵ_{DP}, the single-vertex event selection efficiency ϵ_{1vtx}, and the number of beam crossings with one hard collision, N_{1coll}:

$$N_{\text{DP}} = \frac{\sigma^{\gamma j}}{\sigma_{\text{eff}}} \frac{\sigma^{jj}}{\sigma_{\text{hard}}} N_{\text{1coll}} \, \epsilon_{\text{DP}} \, \epsilon_{\text{1vtx}}. \qquad (5)$$

The ratio of N_{DP} to N_{DI} allows us to obtain the expression for σ_{eff} in the following form:

$$\sigma_{\text{eff}} = \frac{N_{\text{DI}}}{N_{\text{DP}}} \frac{\varepsilon_{\text{DP}}}{\varepsilon_{\text{DI}}} R_{\text{c}} \sigma_{\text{hard}}, \qquad (6)$$

where $R_c \equiv (1/2)(N_{\text{1coll}}/N_{\text{2coll}})(\varepsilon_{\text{1vtx}}/\varepsilon_{\text{2vtx}})$. The $\sigma^{\gamma j}$ and σ^{jj} cross sections do not appear in this ratio and

all the remaining efficiencies for DP and DI events enter only as ratios, resulting in a reduction of the impact of many correlated systematic uncertainties.

Figure 2 shows the possible configurations of signal $\gamma + 3$ jets DP events produced in a single $p\bar{p}$ interaction and having one parton scattering in the final state with a γ and at least one jet, superimposed with another parton scattering into a final state with at least one jet. We define different event topologies as follows. Events in which both jets from the second parton scattering are reconstructed, pass the selection cuts and are selected as the second and third jets, in order of decreasing jet p_T, are defined as Type I. In Type II events, the second jet in the dijet process is either lost due to the finite jet reconstruction efficiency of detector acceptance or takes the fourth position after the jet p_T ordering. We also distinguish Type III events, in which a jet from the second parton interaction becomes the leading jet of the final 3-jets system, although they are quite rare given the p_T range selected for the photon.

The main background for the DP events are single parton (SP) scatterings with hard gluon bremsstrahlung in the initial or final state $qg \to q\gamma gg$, $q\bar{q} \to g\gamma gg$ that give the same $\gamma + 3$ jets signature. They are also shown in Fig. 2. The fraction of DP events is determined in this analysis using a set of variables sensitive to the kinematic configurations of the two independent scatterings of parton pairs (see Secs. V and VI).

The DI events differ from the DP events by the fact that the second parton scattering happens at a separate $p\bar{p}$ collision vertex. The DI events, with the photon and at least one jet from one $p\bar{p}$ collision, and at least one jet from another $p\bar{p}$ collision are shown in Fig. 3 with a similar (to DP) set of DI event types. The background to DI events is due to two-vertex SP events with hard $\gamma + 3$ jets events from one $p\bar{p}$ interaction with an additional soft interaction, i.e. having no reconstructed jets. The diagrams for these non-DI events are also shown in Fig. 3.

III. D0 DETECTOR AND DATA SAMPLES

The D0 detector is described in detail in [17]. Photon candidates are identified as isolated clusters of energy depositions in the uranium and liquid-argon sampling
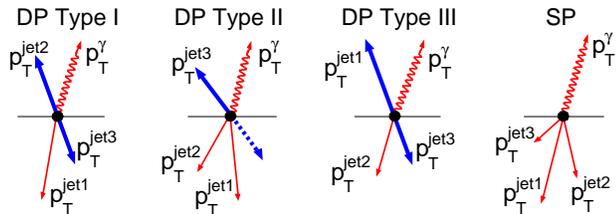
FIG. 2: Diagrams of DP Types I, II, III and SP $\gamma + 3$ jets events. For DP events, the light and bold lines correspond to two separate parton interactions. The dotted line represents unreconstructed jet.
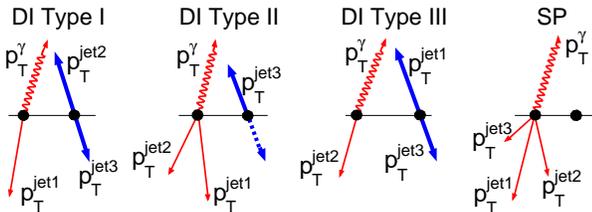

FIG. 3: Diagrams of DI Types I, II, III and SP $\gamma + 3$ jets events. For DI events, the light and bold lines correspond to two separate $p\bar{p}$ interactions. The dotted line represents unreconstructed jet.

calorimeter. The central calorimeter covers the pseudo-rapidity [22] range $|\eta| < 1.1$ and two end calorimeters cover $1.5 < |\eta| < 4.2$. The electromagnetic (EM) section of the calorimeter is segmented longitudinally into four layers and transversely into cells in pseudorapidity and azimuthal angle $\Delta\eta \times \Delta\phi = 0.1 \times 0.1$ (0.05×0.05 in the third layer of the EM calorimeter). The hadronic portion of the calorimeter is located behind the EM section. The calorimeter surrounds a tracking system consisting of silicon microstrip and scintillating fiber trackers, both located within a 2 T solenoidal magnetic field.

The events used in this analysis should first pass triggers based on the identification of high p_T clusters in the EM calorimeter with loose shower shape requirements for photons. These triggers are 100% efficient for $p_T^\gamma > 35$ GeV. To select photon candidates in our data samples, we use the following criteria [19]. EM objects are reconstructed using a simple cone algorithm with a cone size $\mathcal{R} = \sqrt{(\Delta\eta)^2 + (\Delta\phi)^2} = 0.2$. Regions with poor photon identification capability and limited p_T^γ resolution, at the boundaries between calorimeter modules and between the central and endcap calorimeters, are excluded from analysis. Each photon candidate was required to deposit more than 96% of detected energy in the EM section of the calorimeter and to be isolated in the angular region between $\mathcal{R} = 0.2$ and $\mathcal{R} = 0.4$ around the center of the cluster: $(E_{\text{Tot}}^{\text{iso}} - E_{\text{Core}}^{\text{iso}})/E_{\text{Core}}^{\text{iso}} < 0.07$, where $E_{\text{Tot}}^{\text{iso}}$ is overall (EM+hadronic) tower energy in the (η, ϕ) cone of radius $\mathcal{R} = 0.4$ and $E_{\text{Core}}^{\text{iso}}$ is EM tower energy within a radius of $\mathcal{R} = 0.2$. Candidate EM clusters

matched to a reconstructed track are excluded from the analysis. Clusters are matched to a reconstructed track by computing a χ^2 function which evaluates the consistency, within uncertainties, between the reconstructed η and ϕ positions of the cluster and of the closest track extrapolated to the finely-segmented third layer of the EM calorimeter. The corresponding χ^2 probability is required to be $< 0.1\%$. We also require the energy-weighted EM cluster width in the finely-segmented third EM layer to be consistent with that expected for an electromagnetic shower. In addition to the calorimeter isolation, we also apply a track isolation cut, requiring the scalar sum of track transverse momenta in a annulus of $0.05 \leq \mathcal{R} \leq 0.4$ to be less than 1.5 GeV. Jets are reconstructed using the iterative midpoint cone algorithm [23] with a cone size of 0.7. Jets must satisfy quality criteria which suppress background from leptons, photons, and detector noise effects. To reject background from cosmic rays and $W \to \ell\nu$ decay, the missing transverse momentum in the event is required to less than $0.7p_T^\gamma$. All pairs of objects in the event, (photon, jet) or (jet, jet), also are required to be separated in $\eta - \phi$ space by $\Delta\mathcal{R} > 0.7$.

Each event must contain at least one γ in the rapidity region $|y| < 1.0$ or $1.5 < |y| < 2.5$ and at least three jets with $|y| < 3.0$. Events are selected with γ transverse momentum $60 < p_T^\gamma < 80$ GeV, leading (in p_T) jet $p_T > 25$ GeV, while the next-to-leading (second) and third jets must have $p_T > 15$ GeV. The jet transverse momenta are corrected to the particle level. The high p_T^γ scale (i.e. the scale of the first parton interaction) allows a better separation of the first and second parton interactions in momentum space.

Data events with a single $p\bar{p}$ collision vertex, which compose the sample of DP candidates ("1Vtx" sample), are selected separately from events with two vertices which compose the sample of DI candidates ("2Vtx" sample). The collision vertices in both samples are required to have at least three associated tracks and to be within 60 cm of the center of the detector along the beam (z) axis.

The p_T spectrum for jets from dijet events falls faster than that for jets resulting from initial or final state radiation in the $\gamma + $ jets events, and thus DP fractions should depend on the jet p_T [1, 3, 4, 10]. The DP fractions and σ_{eff} are determined in three p_T^{jet2} bins: 15–20, 20–25, and 25–30 GeV. The total numbers of 1Vtx and 2Vtx $\gamma + 3$ jets events remaining in each of the three p_T^{jet2} bins after all selection criteria are given in Table II.

TABLE II: The numbers of selected 1Vtx and 2Vtx $\gamma + 3$ jets events in bins of p_T^{jet2}.

Data	p_T^{jet2} (GeV)		
Sample	$15 - 20$	$20 - 25$	$25 - 30$
1Vtx	2182	3475	3220
2Vtx	2026	2792	2309

IV. DP AND DI MODELS

To study properties of DP and DI events and calculate their fractions in the 1Vtx and 2Vtx samples, respectively, we construct DP and DI models by pairing data events. The DP model is constructed by overlaying in a single event one event of an inclusive sample of $\gamma + \geq 1$ jet events and one event of a sample of inelastic non-diffractive events selected with the minimum bias trigger and a requirement of at least one jet ("MB" sample) [24]. Both samples contain only single-vertex events. The jet p_T from the MB events is recalculated relative to the vertex of the γ+jet event. The resulting mixed events, with jets re-ordered in p_T, are required to pass the $\gamma + 3$ jets event selections described above. This model of DP events, called MixDP, assumes independent parton scatterings, with $\gamma +$ jets and dijet final states, by construction. The mixing procedure is shown schematically in Fig. 4.
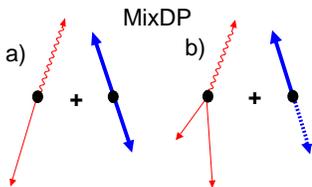
FIG. 4: Description of the mixing procedure used to prepare the MixDP signal sample. Two combinations of mixing $\gamma + 1$ jet and two jets from dijet events (a) and $\gamma + 2$ jets and one jet from dijet events (b) are considered. The dotted line represents a jet failing the selection requirements.

In the DI model, called MixDI, each event is constructed by mixing one event of the $\gamma + \geq 1$ jet sample and one event of the ≥ 1 jet MB sample. Both events are exclusively selected from the two-vertices events sample. In the case of ≥ 2 jets in any component of the MixDI mixture, the first two jets, leading in p_T, are required to originate from the same vertex using the position along the beam axis of the point of closest approach to a vertex for the tracks associated to each jet and a cut on the minimal jet charged particle fraction, as discussed in Appendix B. We consider the two-vertex $\gamma +$ jets and dijet events, components of the MixDI model, to better take into account the underlying energy, coming from the soft interactions of the spectator partons. The amount of this energy is different for single– and two-vertex events and causes a difference in the photon and jet identification efficiencies in the DP and DI events (see Section VII). As a background to the DI events, we consider the two-vertex $\gamma + 3$ jets sample without a hard interaction at the second vertex (Bkg2Vtx sample), obtained by imposing the direct requirement that all three jets originate from the same vertex using the jet track information.

The fractions of Type I (II) events in the MixDP and MixDI samples are the same within 1.5% for each $p_T^{\rm jet2}$ bin and vary for both samples from 26% (73%) at $15 <$ $p_T^{\rm jet2} < 20$ GeV to (14–15)% [(84–86)%] at $25 < p_T^{\rm jet2} <$ 30 GeV. Type III events are quite rare and their fraction does not exceed 1%. The MixDP and MixDI samples have similar kinematic (p_T and η) distributions for the photon and all the jets. They differ only by the amount of energy coming from soft parton interactions in either one or two $p\bar{p}$ collisions, which may affect the photon and the jet selection efficiencies.

V. DISCRIMINATING VARIABLES

A distinctive feature of the DP events is the presence of two independent parton-parton scatterings within the same $p\bar{p}$ collision. We define variables sensitive to the kinematics of DP events, specifically to the difference between the p_T imbalance of the two object pairs in DP and SP $\gamma + 3$ jets events as [4]:

$$\Delta S \equiv \Delta\phi\left(\vec{p}_T(\gamma, i),\ \vec{p}_T(j, k)\right), \qquad (7)$$

where the indices $i, j, k\ (= 1, 2, 3)$ run over the jets in the event. Here $\vec{p}_T(\gamma, i) = \vec{p}_T^{\,\gamma} + \vec{p}_T^{\,\rm jet_i}$ and $\vec{p}_T(j, k) = \vec{p}_T^{\,\rm jet_j} + \vec{p}_T^{\,\rm jet_k}$, where the two object pairs, (γ, jet i) and (jet j, jet k), are selected to give the minimal p_T imbalance. These pairs are found by minimizing S_{p_T}, or $S_{p'_T}$, or S_ϕ defined as

$$S_{p_T} = \frac{1}{\sqrt{2}}\sqrt{\left(\frac{|\vec{p}_T(\gamma, i)|}{\delta p_T(\gamma, i)}\right)^2 + \left(\frac{|\vec{p}_T(j, k)|}{\delta p_T(j, k)}\right)^2}, \qquad (8)$$

$$S_{p'_T} = \frac{1}{\sqrt{2}}\sqrt{\left(\frac{|\vec{p}_T(\gamma, i)|}{|\vec{p}_T^{\,\gamma}| + |\vec{p}_T^{\,i}|}\right)^2 + \left(\frac{|\vec{p}_T(j, k)|}{\left|\vec{p}_T^{\,j}\right| + |\vec{p}_T^{\,k}|}\right)^2}, \qquad (9)$$

$$S_\phi = \frac{1}{\sqrt{2}}\sqrt{\left[\frac{\Delta\phi(\gamma, i)}{\delta\phi(\gamma, i)}\right]^2 + \left[\frac{\Delta\phi(j, k)}{\delta\phi(j, k)}\right]^2}. \qquad (10)$$

In Eq. (10) $\Delta\phi(\gamma, i) = |\pi - \phi(\gamma, i)|$ is the supplement to π of the minimal azimuthal angle between the vectors $\vec{p}_T^{\,\gamma}$ and $\vec{p}_T^{\,\rm jet_i}$, $\phi(\gamma, i)$.

The uncertainties $\delta p_T(\gamma, i)$ in Eq. (8) and $\delta\phi(\gamma, i)$ in Eq. (10) are calculated as root-mean-square values of the $|\vec{p}_T(\gamma, i)|$ and $\Delta\phi(\gamma, i)$ distributions using the signal MixDP sample for each of the three possible pairings. Azimuthal angles and uncertainties for jets j and k are defined analogously to those for the photon and jet i. Any of the S-variables in Eqs. (8)–(10) represents a significance of the pairwise p_T-imbalance. On average, it should be higher for the SP events than for the DP events. Also, each S-variable effectively splits the $\gamma + 3$ jets system into γ+jet and dijet pairs, based on the best pairwise balance.

The two best p_T-balancing pairs, which give the minimum S for each of three variables in Eqs. (8) – (10),

are used to calculate the corresponding ΔS variables, $\Delta S_{p_T}, \Delta S_{p'_T}$ and ΔS_ϕ, according to Eq. (7). The $\Delta S_{p_T}, \Delta S_{p'_T}$ variables are also used in [7, 9], while the ΔS_ϕ is first introduced in this measurement.

Figure 5 illustrates a possible orientation of the transverse momenta vectors of the photon and jets as well as their p_T imbalances vectors, $\vec{P}_T^1$ and $\vec{P}_T^2$, in $\gamma + 3$ jets events. In SP events, the topologies with the two radiation jets emitted close to the leading jet (recoiling against the photon direction in ϕ) are preferred. The resulting peak at $\Delta S = \pi$ is smeared by the effects of additional gluon radiation and detector resolution. For a simple model of DP events, we have exact pairwise balance in p_T and thus ΔS will be undefined. The exact p_T balance in the pairs can be violated due to either detector resolution or additional gluon radiation. Both effects introduce an additional random contribution to the azimuthal angle between the γ+jet and the dijet p_T imbalance vectors, broadening the ΔS distribution.
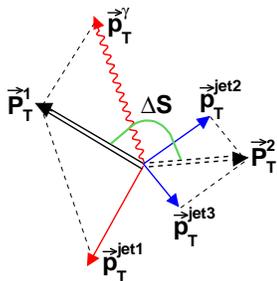
FIG. 5: A possible orientation of photon and jets transverse momenta vectors in $\gamma + 3$ jets events. Vectors $\vec{P}_T^1$ and $\vec{P}_T^2$ are the p_T imbalance vectors of γ+jet and jet-jet pairs. The figure illustrates a general case for the production of $\gamma + 3$ jets +X events.

VI. FRACTIONS OF DP AND DI EVENTS

A. Fractions of DP events

To extract the fractions of DP events, we exploit the difference in the p_T spectrum of DP and radiation jets, mentioned in Sec. III, and consider data in two adjacent p_T^{jet2} intervals: DP-enriched at smaller p_T^{jet2} and DP-depleted at larger p_T^{jet2} [1, 3, 4]. The distribution for each ΔS variable in data (D) can be expressed as a sum of signal (DP) and background (SP) distributions:

$$D_1 = f_1 M_1 + (1 - f_1)B_1 \qquad (11)$$

$$D_2 = f_2 M_2 + (1 - f_2)B_2, \qquad (12)$$

where M_i and B_i stand for the signal MixDP and background distributions, f_i is the DP fraction, $(1 - f_i)$ is the SP fraction, and indices 1, 2 correspond to the DP-enriched and DP-depleted data sets. Multiplying (12) by λK and subtracting from (11) we obtain:

$$D_1 - \lambda K D_2 = f_1 M_1 - \lambda K C f_1 M_2, \qquad (13)$$

where $\lambda = B_1/B_2$ is the ratio of the background distributions, and $K = (1 - f_1)/(1 - f_2)$ and $C = f_2/f_1$ are the ratios of the SP and DP fractions between the DP-enriched and DP-depleted samples, respectively. In contrast to [9], we introduce a factor λ that corrects for the relative difference of ΔS shapes for the SP distributions in adjacent p_T^{jet2} intervals. It is obtained using Monte Carlo (MC) $\gamma + 3$ jets events generated with PYTHIA [25] without multiple parton interactions and with a full simulation of the detector response and is found to be in the range $0.95 - 1.3$ for different bins of ΔS. The factor C is extracted using ratios of the numbers of events in data and MixDP samples in the adjacent bins by

$$C = \left(N_2^{\text{MixDP}}/N_2^{\text{data}}\right) / \left(N_1^{\text{MixDP}}/N_1^{\text{data}}\right), \qquad (14)$$

i.e. without actual knowledge of DP fractions in those bins. Thus, the only unknown parameter in Eq. (13) is the DP fraction f_1. It is obtained from a χ^2 minimization of Eq. (13) using MINUIT [26]. The fit was performed for each pair of p_T^{jet2} bins ($15 - 20/20 - 25$ GeV and $20 - 25/25 - 30$ GeV) and for each of ΔS variables (8)–(10). The DP fractions in the last bin, $25 < p_T^{\text{jet2}} < 30$ GeV, are calculated from $f_2 = C f_1$. The extracted DP fractions are shown in Fig. 6. The DP fractions, av-
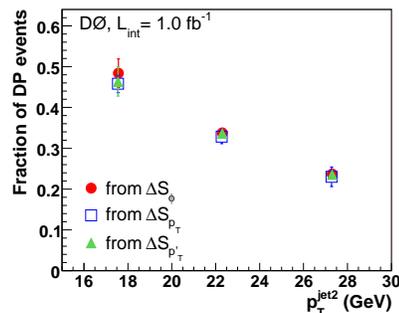

FIG. 6: Fractions of DP events extracted with the ΔS_ϕ , ΔS_{p_T} , and $\Delta S_{p'_T}$ variables in the three p_T^{jet2} intervals.

eraged over the three ΔS variables (with uncertainties), are summarized in Table III. The location of the points in Fig. 6 corresponds to the mean p_T^{jet2} for the DP model in a given bin. They are also shown in Table III as $\langle p_T^{\text{jet2}} \rangle$. The uncertainties are mainly caused by the statistics of the data and MixDP samples (used in the fitting) and partially by the determination of λ $(2 - 5)\%$.

TABLE III: Fractions of DP events in the three p_T^{jet2} bins.

p_T^{jet2} GeV	$\langle p_T^{\text{jet2}} \rangle$ (GeV)	f_{DP}
$15 - 20$	17.6	0.466 ± 0.041
$20 - 25$	22.3	0.334 ± 0.023
$25 - 30$	27.3	0.235 ± 0.027

Since each component of a MixDP signal event may contain two jets, where one jet may be caused by an
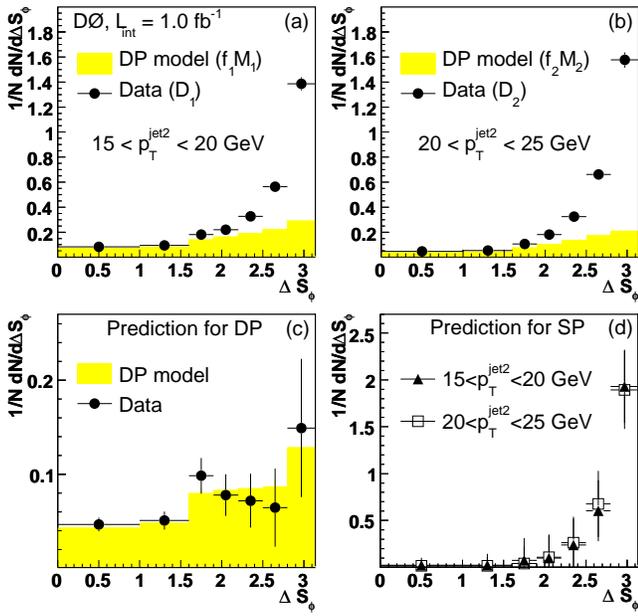
FIG. 7: Results of the two datasets fit for the ΔS_ϕ variable for the combination of two p_T^{jet2} bins $15 - 20$ GeV and $20 - 25$ GeV. (a) and (b) show distributions for data (points) and the DP model (shaded area); (c) shows the prediction for DP from data (points), corrected to remove SP contribution, and the DP model (shaded area) as a difference between the corresponding distributions of (a) and (b); (d) shows the extracted SP distributions in the two bins. The error bars in (a) and (b) are only statistical, while in (c) and (d) they represent total (statistic and systematic) uncertainty.

FIG. 8: Same as in Fig. 7 but for the other combination of p_T^{jet2} bins, $20 - 25$ GeV and $25 - 30$ GeV.

additional parton interaction, the MixDP sample should simulate the properties of the double plus triple parton (TP) interactions (DP+TP), and thus the fractions in Table III take into account a contribution from triple interactions as well. In this sense, the DP cross section calculated using Eqs. (1) and (6) is inclusive [27, 28].

Figure 7 shows tests of the fit results for f_1 using the ΔS_ϕ variable for the combination of two p_T^{jet2} bins, $15 - 20$ GeV and $20 - 25$ GeV. Figure 7(a) show the ΔS_ϕ distributions for the DP-enriched data set in data (D_1) and the MixDP sample (M_1) weighted with its fraction f_1. Figure 7(b) shows analogous distributions for the DP-depleted dataset: data (D_2) and the MixDP sample (M_2) weighted with its fraction f_2. It can be concluded from the two distributions that the regions of small ΔS_ϕ $(\lesssim 1.5)$ is mostly populated by signal events with two independent hard interactions. Figure 7(c) shows the difference between the data distributions of Figs. 7(a) and 7(b), corrected to remove the SP contribution by the factor λK (the factor λ corrects for the relative difference of the ΔS_ϕ shapes and K corrects for the difference in the SP fractions in the two adjacent p_T^{jet2} bins) [left side of Eq. (13)] and compared to the MixDP prediction [right side of Eq. (13)]. As expected, the difference is always positive since the fractions of DP events drop with p_T^{jet2}. The DP model provides an adequate description of the
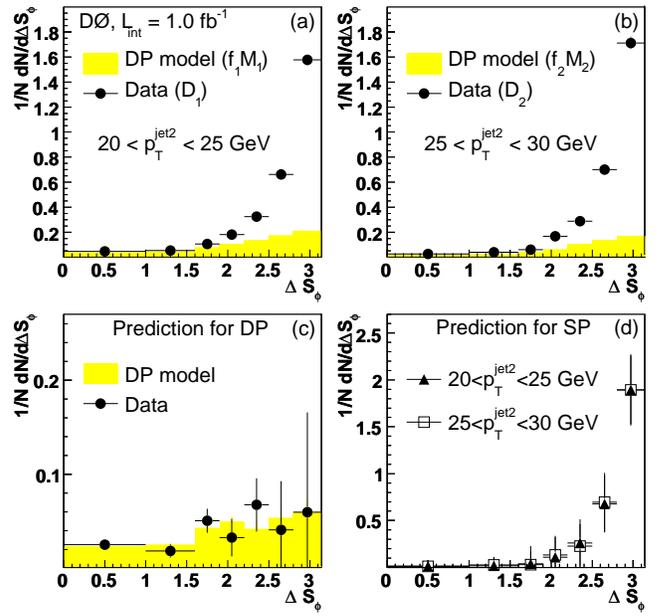
data. In Fig. 7(d) we extract the SP distributions by subtracting the estimated DP contributions from the data: $(D_1 - f_1 M_1)/(1 - f_1)$ for the DP-enriched data set and $(D_2 - f_2 M_2)/(1 - f_2)$ for the DP-depleted data sets. Figure 8 shows the analogous test of the fit results for the other pair of p_T^{jet2} bins, $20 - 25$ GeV and $25 - 30$ GeV.

Predictions for SP events are obtained using PYTHIA. The $\Delta S_{p_T'}$ distribution for $\gamma + 3$ jets events simulated with initial and final state radiation (ISR and FSR) and without multiple parton interactions (MPI) is shown in Fig. 9 for the interval $15 < p_T^{\text{jet2}} < 20$ GeV. Since the $\vec{p}_T$ imbalance of the two additional jets should compensate the $\vec{p}_T$ imbalance of the "γ+leading jet" system, the $\Delta S_{p_T'}$ distribution is shifted towards π. This distributions shows good agreement with the results for the SP sample shown in Fig. 7(d). The DP $\gamma + 3$ jets events are
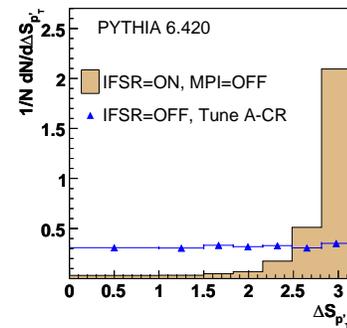

FIG. 9: $\Delta S_{p_T'}$ distributions for $\gamma + 3$ jets events simulated using PYTHIA with ISR/FSR but with MPI switched off (shaded region), as well as for $\gamma + 3$ jets events without ISR/FSR but MPI switched on using Tune A-CR (triangle markers). The bin $15 < p_T^{\text{jet2}} < 20$ GeV is considered.

also simulated without ISR and FSR and using the MPI model corresponding to the PYTHIA parameters Tune A-CR [25]. In this case, the two subleading jets may originate only from the second parton interaction (as in DP events of Type I, see Fig. 2). As expected, the $\Delta S_{p'_T}$ distribution for these events is uniform, since the two p_T balance vectors for the two systems, $\gamma + \text{jets}$ and dijets, are independent from each other.

Another source of background to the single-vertex $\gamma + 3$ jets DP events is caused by double $p\bar{p}$ collisions close to each other along the beam direction, for which a single vertex is reconstructed. This was estimated separately and found to be negligible with a probability $< 10^{-3}$.

B. Fractions of DI events

The DI fractions, f_{DI}, are extracted by fitting the shapes of the ΔS distributions of the MixDI signal and Bkg2Vtx background samples to that for the 2Vtx data using the technique described in [29]. Uncertainties are mainly caused by the fitting procedure and by building Bkg2Vtx and MixDI (in case of Type I events) models. To estimate the uncertainty due to the Bkg2Vtx or MixDI models, we vary a cut on the minimal jet charged particle fraction (see Appendix B) from 0.5 to 0.75. The fitted f_{DI} in this case varies in different p_T^{jet2} bins within $(3-10)\%$, which is taken as the uncertainty. The final f_{DI} values with total uncertainties are 0.189 ± 0.029 for $15 < p_T^{\text{jet2}} < 20$ GeV, 0.137 ± 0.027 for $20 < p_T^{\text{jet2}} < 25$ GeV, and 0.094 ± 0.025 for $25 < p_T^{\text{jet2}} < 30$ GeV. The relative f_{DI} uncertainties grow with increasing p_T^{jet2}. This is caused by a decreasing probability for a jet to originate from a second $p\bar{p}$ collision vertex. As a consequence, the sensitivity to DI events in the 2Vtx data sample becomes smaller.

Figure 10 shows the ΔS_ϕ distributions for the two-vertex $\gamma + 3$ jets events selected in three p_T^{jet2} intervals, $15-20$ GeV, $20-25$ GeV and $25-30$ GeV, for the DI model (MixDI) and the total sum of MixDI and Bkg2Vtx distributions, weighted with the DI fraction, and compared to 2Vtx data. The weighted sums of the signal and background samples reproduce the shapes of the data distributions.

VII. DP AND DI EFFICIENCIES, R_c AND σ_{hard}

A. Ratio of photon and jet efficiencies in DP and DI events

The selection efficiencies for DP and DI events enter Eq. (6) only as ratios, canceling many common correction factors and correlated systematic uncertainties. The DP and DI events differ from each other by the number of $p\bar{p}$ collision vertices (one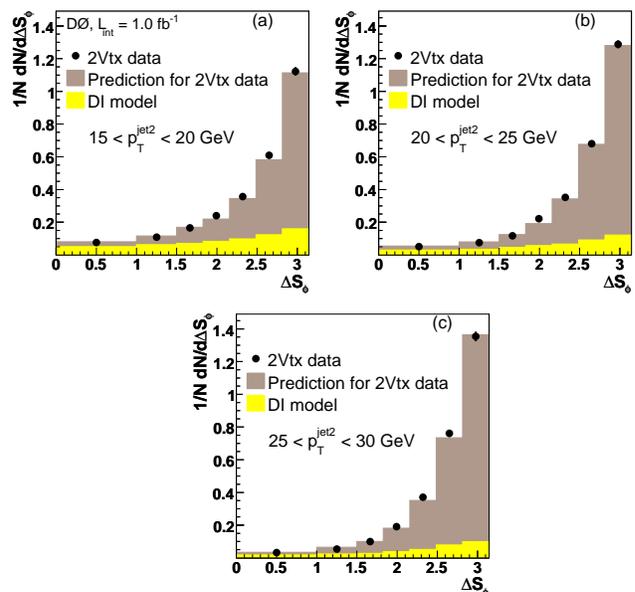 vs. two), and therefore their selection efficiencies ε_{DI} and ε_{DP} may differ due to

FIG. 10: ΔS_ϕ distributions for two-vertex $\gamma + 3$ jets events in the three p_T^{jet2} intervals: (a) $15-20$ GeV, (b) $20-25$ GeV and (c) $25-30$ GeV. MixDI and the total sum of the MixDI and Bkg2Vtx distributions (shaded histograms) are weighted with their fractions found from the fit, compared to 2Vtx data (black points). The shown uncertainties are only statistical.

different amounts of soft unclustered energy in the single and double $p\bar{p}$ collision events. This could lead to a difference in the jet reconstruction efficiencies, due to the different probabilities of passing the jet selection requirement $p_T > 6$ GeV (applied during jet reconstruction) and different photon selection efficiencies, due to different amount of energy in the track and calorimeter isolation cones around the photon.

To estimate these efficiencies, we use $\gamma + \text{jets}$ and dijet MC events and also MixDI and MixDP data samples. The MC events are generated with PYTHIA [25] and processed through a GEANT-based [30] simulation of the D0 detector response. In order to accurately model the effects of multiple proton-antiproton interactions and detector noise, data events from random $p\bar{p}$ crossings are overlaid on the MC events using data from the same time period as considered in the analysis. These MC events are then processed using the same reconstruction code as for the data. We also apply additional smearing to the reconstructed photon and jet p_T so that the measurement resolutions in MC match those in data. The MC events are preselected with the vertex cuts and split into the single– and two-vertex samples.

The efficiencies for the photon selection criteria are estimated using $\gamma + \text{jets}$ MC events. We found that the ratio of photon efficiencies in single-vertex (ε_{1v}^γ) to that in two-vertex samples (ε_{2v}^γ) does not have a noticeable dependence on p_T^{jet2} and can be taken as $\varepsilon_{1v}^\gamma / \varepsilon_{2v}^\gamma = 0.96 \pm 0.03$. The purity of $\gamma + \text{jets}$ events in the interval of $60 < p_T^\gamma < 80$ GeV in data is expected to be about 75% [19], and the remaining events are mostly dijet events with

one jet misidentified as photon. An analogous analysis of the MC dijet events gives the ratio of the efficiencies for jets to be misidentified as photons equal to 0.99 ± 0.06, which does not change the $\varepsilon_{1v}^{\gamma}/\varepsilon_{2v}^{\gamma}$ value found with the signal γ + jets sample.

The ratio of jet efficiencies is calculated in two steps. First, the efficiencies are estimated with respect to a requirement to have at least three jets with $p_T^{jet1} > 25$ GeV, $p_T^{jet2} > 15$ GeV, and $p_T^{jet3} > 15$ GeV. These efficiencies are calculated using MC γ + jets and dijet events mixed according to the fractions of the three main MixDP and MixDI event types, described in Sec. IV. The ratio of efficiencies for other jet selections (e.g. to get into the p_T^{jet2} interval and satisfy $\Delta\mathcal{R}$ and jet rapidity selections) has been calculated using MixDP and MixDI signal data samples. The total ratio of DP/DI jet efficiencies is found to be stable for all p_T^{jet2} bins and equal to 0.93 with $\sim 5\%$ uncertainty. Thus, the overall ratio of photon and jet DP/DI selection efficiencies $\varepsilon_{DP}/\varepsilon_{DI}$ is about 0.90 with uncertainties in the three p_T^{jet2} bins varying within $(5.6 - 6.5)\%$.

B. Vertex efficiencies

The vertex efficiency ε_{1vtx} (ε_{2vtx}) corrects for the single (double) collision events that are lost in the DP (DI) candidate sample due to the single (double) vertex cuts ($|z_{vtx}| < 60$ cm and ≥ 3 tracks). The ratio $\varepsilon_{1vtx}/\varepsilon_{2vtx}$ is calculated from the data and found to be 1.08 ± 0.01 for all p_T^{jet2} bins. The probability to miss a hard interaction event with at least one jet with $p_T > 15$ GeV due to a non-reconstructed vertex is calculated in γ + jets and minimum bias data and found to be $(0.2 - 0.4)\%$. The probability to have an additional reconstructed vertex, passing the vertex selection requirements, is estimated separately using γ + jets and dijet MC events with at least one reconstructed jet with $p_T > 15$ GeV and found to be less than 0.3%.

C. Calculating σ_{hard}, N_{1coll} and N_{2coll}

The numbers of expected events with one (N_{1coll}) and two (N_{2coll}) $p\bar{p}$ collisions resulting in hard interactions are calculated from the known instantaneous luminosity spectrum of the collected data (L_{inst}), the frequency of beam crossings (f_{cross}) for the Tevatron [17], and the hard $p\bar{p}$ interaction cross section (σ_{hard}).

The value of σ_{hard} at $\sqrt{s} = 1.96$ TeV is obtained in the following way. We use the inelastic cross section calculated at $\sqrt{s} = 1.96$ TeV, $\overline{\sigma}_{inel}(1.96$ TeV$) = 60.7 \pm 2.4$ mb [31], found from averaging the inelastic cross sections measured by the CDF [32] and E811 [33] Collaboration at $\sqrt{s} = 1.8$ TeV and extrapolated to 1.96 TeV. To calculate single diffractive (SD) and double diffractive (DD) cross sections at

$\sqrt{s} = 1.96$ TeV, $\sigma_{SD}(1.96$ TeV$)$ and $\sigma_{DD}(1.96$ TeV$)$, we use SD and DD cross sections measured at $\sqrt{s} = 1.8$ TeV ($\sigma_{SD}(1.8$ TeV$) = 9.46 \pm 0.44$ mb [32] and $\sigma_{DD}(1.8$ TeV$) = 6.32 \pm 0.03(stat) \pm 1.7(syst)$ mb) [34] and extrapolate them to $\sqrt{s} = 1.96$ TeV using the slow asymptotic behaviour predicted in [35]. We find

$$\sigma_{hard}(1.96 \text{ TeV}) = \overline{\sigma}_{inel}(1.96 \text{ TeV}) - \sigma_{SD}(1.96 \text{ TeV})$$
$$-\sigma_{DD}(1.96 \text{ TeV}) = 44.76 \pm 2.89 \text{ mb. (15)}$$

We also do analogous estimates by calculating first σ_{hard} at $\sqrt{s} = 1.8$ TeV and then extrapolating it to $\sqrt{s} = 1.96$ TeV using [35]. This method results in $\sigma_{hard}(1.96$ TeV$) = 43.85 \pm 2.63$ mb which agrees well with Eq. (15).

In each bin of the L_{inst} spectrum, we calculate the average number of hard $p\bar{p}$ interactions $\langle n \rangle = (L_{inst}/f_{cross})\sigma_{hard}$ and then N_{1coll} and N_{2coll} are determined from $\langle n \rangle$ using Poisson statistics. Summing over all L_{inst} bins, weighted with their fractions, we get $N_{1coll}/(2N_{2coll}) = 1.169$ and thus $R_c\sigma_{hard} = 56.45 \pm 0.88$ mb. Here we take into account that R_c and σ_{hard} enter Eq. (6) for σ_{eff} as a product. Any increase of σ_{hard} leads to an increase of $\langle n \rangle$ and, as a consequence, to a decrease in R_c, and vice versa. Specifically, while the found value of σ_{hard} has a 6.5% relative uncertainty, the product $R_c\sigma_{hard}$ has approximately 2% uncertainty.

VIII. RESULTS

A. Effective cross section

The calculation of σ_{eff} is based on Eq. (6) of Sec. I. The numbers N_{DP} and N_{DI} in each p_T^{jet2} bin are obtained from the numbers of the 1Vtx and 2Vtx $\gamma + 3$ jets events in Table II, multiplying them by f_{DP} and f_{DI}. The determination of all other components of Eq. (6) are described in Sec. VII. The resulting values of σ_{eff} with total uncertainties (statistical and systematic are summed in quadrature) are shown in Fig. 11 and given in Table IV for the three p_T^{jet2} bins. The location of the points in Fig. 11 corresponds to the mean p_T^{jet2} for the DP model in a given bin (the mean p_T^{jet2} values for DI model are the same within 0.15 GeV). These values are also shown in Table IV. Table V summarizes the main sources of uncertainties for each p_T^{jet2} bin. The main systematic uncertainties are related to the determinations of the DI fractions (dominant uncertainty), DP fractions, the $\varepsilon_{DP}/\varepsilon_{DI}$ ratio, jet energy scale (JES), and $R_c\sigma_{hard}$, giving a total systematic uncertainty of $(20.5 - 32.2)\%$.

TABLE IV: Effective cross section σ_{eff} in the three p_T^{jet2} bins.

p_T^{jet2} GeV	$\langle p_T^{jet2} \rangle$ (GeV)	σ_{eff} (mb)
$15 - 20$	17.6	18.2 ± 3.8
$20 - 25$	22.3	16.3 ± 3.7
$25 - 30$	27.3	13.9 ± 4.5

TABLE V: Systematic (δ_{syst}), statistic (δ_{stat}) and total δ_{total} uncertainties (in %) for σ_{eff} in the three p_T^{jet2} bins.

p_T^{jet2}	Systematic uncertainty sources					δ_{syst}	δ_{stat}	δ_{total}
(GeV)	f_{DP}	f_{DI}	$\varepsilon_{\text{DP}}/\varepsilon_{\text{DI}}$	JES	$R_c\sigma_{\text{hard}}$	(%)	(%)	(%)
$15-20$	7.9	17.1	5.6	5.5	2.0	20.5	3.1	20.7
$20-25$	6.0	20.9	6.2	2.0	2.0	22.8	2.5	22.9
$25-30$	10.9	29.4	6.5	3.0	2.0	32.2	2.7	32.3

The measured σ_{eff} values in the different p_T^{jet2} bins agree with each other within their uncertainties, however a slow decrease with p_T^{jet2} can not be excluded. The σ_{eff} value averaged over the three p_T^{jet2} bins is

$$\sigma_{\text{eff}}^{\text{ave}} = 16.4 \pm 0.3(\text{stat}) \pm 2.3(\text{syst}) \ \text{mb}. \qquad (16)$$
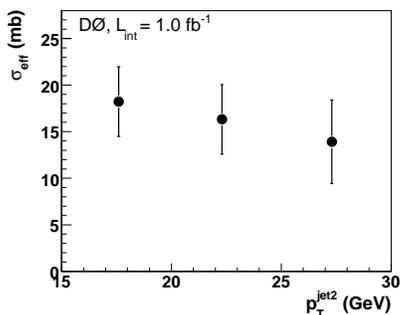

FIG. 11: Effective cross section σ_{eff} (mb) measured in the three p_T^{jet2} intervals.

B.   Models of parton spatial density

In this section we study the limits that can be obtained on the parameters of three phenomenological models of parton spatial density using the measured effective cross section (16). In the discussion below we follow a simple classical approach. For a given parton spatial density inside the proton or antiproton $\rho(r)$, one can define a (time-integrated) overlap $\mathcal{O}(\beta)$ between the parton distributions of the colliding nucleons as a function of the impact parameter β [10]. The larger the overlap (i.e. smaller β), the more probable it is to have at least one parton interaction in the colliding nucleons. The single hard scattering cross sections (for example, $\gamma+$jets or dijet production) should be proportional to $\mathcal{O}(\beta)$ and the cross section for the double parton scattering is proportional to the squared overlap, both integrated over all impact parameters β [28, 36]:

$$\sigma_{\text{eff}} = \frac{[\int_0^\infty \mathcal{O}(\beta) \ 2\pi\beta \ \text{d}\beta]^2}{\int_0^\infty \mathcal{O}(\beta)^2 \ 2\pi\beta \ \text{d}\beta}. \qquad (17)$$

First, we consider the "solid sphere" model with a constant density inside the proton radius r_p. In this model, the total hard scattering cross section can be written as $\sigma_{\text{hard}} = 4\pi r_p^2$ and $\sigma_{\text{eff}} = \sigma_{\text{hard}}/f$. Here f is the geometrical enhancement factor of the DP cross section. It is obtained by solving Eq. (17) for two overlapping spheres with a boundary conditions that the parton density $\rho(r) = \text{constant}$ for $r \leq r_p$ and $\rho(r) = 0$ for $r > r_p$ and found to be $f = 2.19$. The role of the enhancement factor can be seen better if we rewrite Eq. (1) as $\sigma_{\text{DP}} = f\sigma_{\text{A}}\sigma_{\text{B}}/\sigma_{\text{hard}}$. The harder the single-parton interaction is the more it is biased towards the central hadron-hadron collision with a small impact parameter, where we have a larger overlap of parton densities and, consequently, higher probability for a second parton interaction [5]. Using the measured σ_{eff}, for the solid sphere model we extract the proton radius $r_p = 0.53 \pm 0.06$ fm and proton rms-radius $R_{\text{rms}} = 0.41 \pm 0.05$ fm. The latter is obtained from averaging r^2 as $R_{\text{rms}}^2 \equiv \int_0^\infty r^2 4\pi r^2 \rho(r) dr = 4\pi \int_0^\infty \rho(r) r^4 dr$ [37]. The results are summarized in the line "Solid Sphere" of Table VI. The Gaussian model with $\rho(r) \propto e^{-r^2/2a^2}$ and exponential model with $\rho(r) \propto e^{-r/b}$ have been also tested. The relationships between the scale parameter (r_p, a or b) and rms-radius for all the models are given in Table VI. The relationships between the effective cross section σ_{eff} and parameters of the Gaussian and exponential models are taken from [38], neglecting the terms that represent correlations in the transverse space. The scale parameters and rms-radii for both models are also given in Table VI. In spite of differences in the models, the proton rms-radii are in good agreement with each other, with average values varied as $0.41-0.47$ and with about 12% uncertainty. On the other hand, having obtained rms-radius from other sources (for example, [39]) and using the measured σ_{eff}, the size of the transverse correlations [38] can be estimated.

IX.   SUMMARY

We have analyzed a sample of $\gamma + 3$ jets events collected by the D0 experiment with an integrated luminosity of about 1 fb^{-1} and determined the fraction of events with hard double parton scattering occurring in a single $p\bar{p}$ collision at $\sqrt{s} = 1.96$ TeV. These fractions are measured in three intervals of the second (ordered in p_T) jet transverse momentum p_T^{jet2} and vary from 0.466 ± 0.041 at $15 \leq p_T^{\text{jet2}} \leq 20$ GeV to 0.235 ± 0.027 at $25 \leq p_T^{\text{jet2}} \leq 30$ GeV.

In the same three p_T^{jet2} intervals, we calculate an ef-

TABLE VI: Parameters of parton spatial density models calculated from measured $\sigma_{\rm eff}$.

Model for density	$\rho(r)$	$\sigma_{\rm eff}$	$R_{\rm rms}$	Parameter (fm)	$R_{\rm rms}$ (fm)
Solid Sphere	Constant, $r < r_p$	$4\pi r_p^2/2.2$	$\sqrt{3/5}r_p$	0.53 ± 0.06	0.41 ± 0.05
Gaussian	$e^{-r^2/2a^2}$	$8\pi a^2$	$\sqrt{3}a$	0.26 ± 0.03	0.44 ± 0.05
Exponential	$e^{-r/b}$	$28\pi b^2$	$\sqrt{12}b$	0.14 ± 0.02	0.47 ± 0.06

fective cross section $\sigma_{\rm eff}$, a process-independent scale parameter which provides information about the parton spatial density inside the proton and define the rate of double parton events. The measured $\sigma_{\rm eff}$ values agree for the three $p_T^{\rm jet2}$ intervals with an average $\sigma_{\rm eff}^{\rm ave} = 16.4 \pm 0.3({\rm stat}) \pm 2.3({\rm syst})$ mb. We note that this average value is in the range of those found in previous measurements [7–9] performed at different parton interaction energy scales, and may indicate stable behavior of $\sigma_{\rm eff}$ with respect to the considered energy scales.

Using the measured $\sigma_{\rm eff}$ we have calculated scale parameters and rms-radii of the proton for three models of the parton matter distribution.

Acknowledgements

X. APPENDIX A

In this measurement we assume that the two parton interactions in the DP $\gamma + 3$ jets events can be considered to be independent from each other. Possible correlation may appear both in momentum space, since the two interactions have to share the same proton momentum, and at the fragmentation stage.

In the hypothesis of two independent scatterings, the kinematic properties of SP dijet events should be very similar to those produced in the second parton interaction in the DP $\gamma + 3$ jets events. We compare the p_T and η distributions for the two cases using the PYTHIA event generator, which includes momentum and flavor correlations among the partons participating in MPI. It also provides the possibility of choosing different MPI mod-
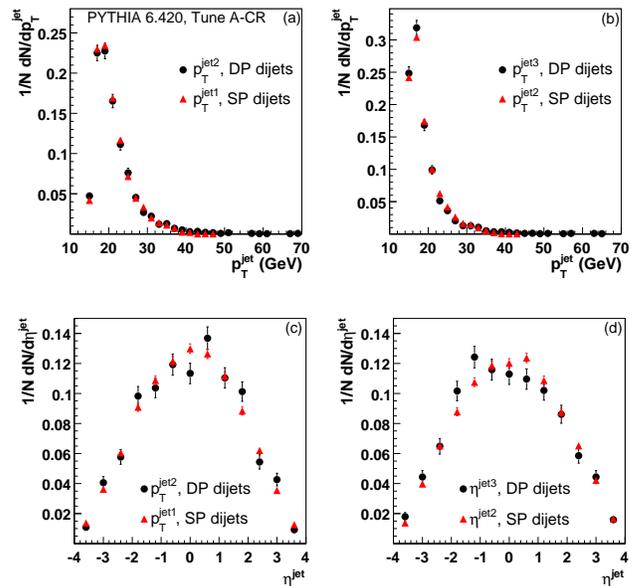

FIG. 12: Comparison of dijet final states in SP (triangles) and in $\gamma + 3$ jets DP events (black circles): (a) and (c) show comparisons of the p_T and η distribution of the second (ordered in p_T) jet in $\gamma + 3$ jets DP events with the first jet from the SP dijet events; (b) and (d) show comparisons of the p_T and η distribution of the third jet in $\gamma + 3$ jets DP events with the second jet from the SP dijet events. Both types of events are generated without ISR and FSR effects but with MPI Tune A-CR.

els. In our comparison we use the PYTHIA parameters Tune A-CR, which is usually considered as an example of a model with a strong color reconnection with an extreme prediction for track multiplicities and/or average hadron p_T [40]. As a model for the DP events, we simulate $\gamma + 3$ jets events using Tune A-CR but with ISR and FSR effects turned off and applied all selection criteria as described in Sec. III. This configuration of the event generator guarantees that the two jets produced in addition to the leading jet (and γ) in the $\gamma + 3$ jets final state arise only from additional parton interactions. The ΔS distribution for these events is shown in Fig. 9 (by triangles). The SP dijets events are also generated without ISR and FSR. Figure 12(a) compares the p_T spectra of the first (in p_T) jet from the second partonic collision in DP events (second jet in $\gamma + 3$ jets events) and the first jet in the SP dijet events, while Fig. 12(b) make analogous comparisons of the next (in p_T) jet in both event types. Figures 12(c) and 12(d) compare the η distributions of

these jets. We can see good agreement between the kinematics of jets produced in the second parton interaction and those from the regular SP dijet events. Analogous comparisons were performed using Tunes A and S0 with similar good agreement. This indicates the absence of visible correlations between the two DP scatterings with our selection criteria.

XI. APPENDIX B

In building signal and background DI models in Sec. IV, we take into account information about tracks associated with jets. We use two algorithms. In the first, we consider all tracks inside a jet radius ($\mathcal{R} = 0.7$ in our case) and calculate the p_T-weighted position in z of all the tracks ("jet$_-z$"). Here the track z position is calculated at the point of closest approach of this track to the beam (z) axis. For each jet in the 2Vtx data sample (Sec. III) we can estimate the distance between the jet$_-z$ and the $p\bar{p}$ vertex closest in z, $\Delta z(\text{Vtx, jet}_i)$. These dis-

tributions are shown in Fig. 13 for each jet in the $\gamma+3$ jets 2Vtx sample. About (95–96)% [(97–99%)] of events have $\Delta z(\text{Vtx, jet}_i) < 1.5 \ (2.0)$ cm.

We also use an algorithm that is based on a jet charged particle fraction (CPF) and define a discriminant which measures the probability that a given jet originates from a particular vertex (a jet, having originated from a vertex, may still have tracks coming from another vertex). The CPF discriminant is based on the fraction of charged transverse energy in each jet i (in the form of tracks) originating from each identified vertex j in the event:

$$\text{CPF}(\text{jet}_i, \text{Vtx}_j) = \frac{\sum_k p_T(\text{trk}_k^{\text{jet}_i}, \text{Vtx}_j)}{\sum_n \sum_l p_T(\text{trk}_l^{\text{jet}_i}, \text{Vtx}_n)}. \quad (18)$$

To confirm that a given jet originate from a vertex, we require $\Delta z < 2.0$ and CPF > 0.5. These requirements being applied to two (or three) jets in the 2Vtx events allow to build the signal and background DI models described in Section IV.

[a] Visitor from Augustana College, Sioux Falls, SD, USA.
[b] Visitor from The University of Liverpool, Liverpool, UK.
[c] Visitor from SLAC, Menlo Park, CA, USA.
[d] Visitor from ICREA/IFAE, Barcelona, Spain.
[e] Visitor from Centro de Investigacion en Computacion - IPN, Mexico City, Mexico.
[f] Visitor from ECFM, Universidad Autonoma de Sinaloa, Culiacán, Mexico.
[g] Visitor from Universität Bern, Bern, Switzerland.

[1] P.V. Landshoff and J.C. Polkinghorne, Phys. Rev. D **18**, 3344 (1978).
[2] C. Goebel, F. Halzen, and D.M. Scott, Phys. Rev. D **22**, 2789 (1980).
[3] N. Paver and D. Treleani, Nuovo Cimento A **70**, 215 (1982); L. Ametller, N. Paver, and D. Treleani, Phys. Lett. B **169**, 289 (1986).
[4] B. Humpert, Phys. Lett. B **131**, 461 (1983); B. Humpert and R. Odorico, Phys. Lett. B **154**, 211 (1985).
[5] T. Sjöstrand, Fermilab Report No. FERMILAB-Pub-85/119-T, 1985; T. Sjöstrand and M. van Zijl, Phys. Rev. D **36**, 2019 (1987).
[6] T. Akesson *et al.* (AFS Collaboration), Z. Phys. C **34**, 163 (1987).
[7] J. Alitti *et al.* (UA2 Collaboration), Phys. Lett. B **268**, 145 (1991).
[8] F. Abe *et al.* (CDF Collaboration), Phys. Rev. D **47**, 4857 (1993).
[9] F. Abe *et al.* (CDF Collaboration), Phys. Rev. Lett. **79**, 584 (1997); Phys. Rev. D **56**, 3811 (1997).
[10] T. Sjöstrand and P. Z. Skands, JHEP **0403**, 053 (2004).
[11] G. Calucci and D. Treleani, Phys. Rev. D **60**, 054023 (1999).
[12] V.L. Korotkikh and A.M. Snigirev, Phys. Lett. B **594**, 171 (2004).
[13] J.R. Gaunt and W.J. Stirling, Cavendish-HEP-09-20, arXiv:0910.4347 [hep-ph] (2009).
[14] T. Sjöstrand and P. Z. Skands, Eur. Phys. J. C **39**, 129 (2005).
[15] A. Del Fabbro, D. Treleani, Phys. Rev. D **61**, 077502 (2000); Phys. Rev. D **66**, 074012 (2002).
[16] M.Y Hussein, Nucl. Phys. Proc. Suppl. **174**, 55 (2007); arXiv:0710.0203 [hep-ph].
[17] V.M. Abazov *et al.* (D0 Collaboration), Nucl. Instrum. Methods Phys. Res. A **565**, 463 (2006).
[18] M. Drees, T. Han, Phys. Rev. Lett. **77**, 4142 (1996).
[19] V.M. Abazov *et al.* (D0 Collaboration), Phys. Lett. B **666**, 435 (2008); Phys. Rev. Lett. **102**, 192002 (2009).
[20] B. Abbott *et al.* (D0 Collaboration), Phys. Lett. B **440**, 189 (1998); B. Abbott *et al.* (D0 Collaboration), Phys. Lett. B **531**, 52 (2002); V. Abazov *et al.* (D0 Collaboration), Phys. Lett. B **574**, 169 (2003).
[21] Rapidity is defined as $y = -(1/2)\ln[(E+p_Z)/(E-p_Z)]$, where E is the energy and p_Z is the momentum component along the proton beam direction.
[22] Pseudorapidity η is defined as $\eta = -\ln[\tan(\theta/2)]$, where θ is the polar angle with respect to the proton beam direction.
[23] G.C. Blazey *et al.*, arXiv:hep-ex/0005012 (2000).
[24] The MB data are collected by requiring only a beam crossing and a coincident signal in the two luminosity monitors located at $2.7 < |\eta| < 4.4$ in pseudorapidity [17].
[25] T. Sjöstrand *et al.*, JHEP **05**, 026 (2006).
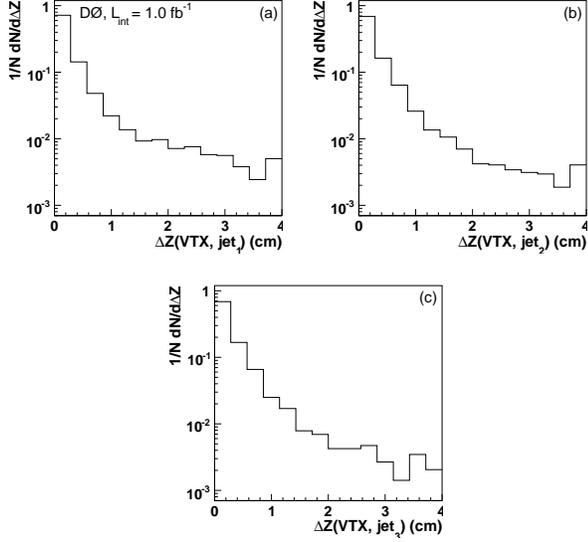[26] F. James, CERN Program Library Long Writeup D506

FIG. 13: Normalized distribution of the number of events as a function of the distance along the z-axis between jet$\_z$ (see text) and the $p\bar{p}$ vertex closest in z-position for the (a) first, (b) second and (c) third jets in the 2Vtx data sample.

(1994).

[27] It differs from [9], where the measured inclusive double parton fractions are corrected for the fraction of triple parton interactions, what makes $\sigma_{\rm eff}$ and then double parton cross section exclusive [28].

[28] D. Treleani, Phys. Rev. D **76**, 076006 (2007).

[29] R. Barlow and C. Beeston, Comput. Phys. Commun. **77**, 219 (1993).

[30] R. Brun and F. Carminati, CERN Program Library Long Writeup W5013 (1993).

[31] S. Klimenko *et al*, Fermilab-FN-0741 (2003).

[32] F. Abe *et al.* (CDF Collaboration), Phys. Rev. D **50**, 5550 (1994).

[33] C. Avila *et al.* (E811 Collaboration), Phys. Lett. B **445**, 419 (1999).

[34] T. Affolder *et al.* (CDF Collaboration), Phys. Rev. Lett. **87**, 141802 (2001).

[35] G.A. Schuler and T. Sjöstrand, Phys. Rev. D **49**, 2257 (1994).

[36] D. Brown, Ph.D. thesis, Harvard University, 1989.

[37] R. Hoftstadter, Rev. Mod. Phys. **28**, 214 (1956).

[38] G. Calucci and D. Treleani, Phys. Rev. **D79**, 074013 (2009).

[39] A.V. Belitsky and A.V. Radyushkin, Phys. Rept. **418**, 1–385 (2005).

[40] D. Wicke and P.Z. Skands, arXiv:0807.3248 [hep-ph] (Fig.3).